Kinetically Controlled SideWall Functionalization of Carbon Nanotubes by Nitric Acid Oxidation

ARTICLE *in* THE JOURNAL OF PHYSICAL CHEMISTRY C · MAY 2008

Impact Factor: 4.77 · DOI: 10.1021/jp711975a

5 AUTHORS, INCLUDING:

Han-Gang Yu
West Virginia University
160 PUBLICATIONS **3,060** CITATIONS
SEE PROFILE

Feng Peng
South China University of Technology
187 PUBLICATIONS **3,413** CITATIONS
SEE PROFILE

Hao Wang
University of California, Santa Barbara
463 PUBLICATIONS **5,261** CITATIONS
SEE PROFILE

CHEMISTRY
A EUROPEAN JOURNAL

ChemPubSoc
Europe

DOI: 10.1002/chem.201300676

Mechanistic Insight into the Catalytic Oxidation of Cyclohexane over Carbon Nanotubes: Kinetic and In Situ Spectroscopic Evidence

Xixian Yang,[a] Hongjuan Wang,[a] Jing Li,[b] Wenxu Zheng,[b] Rong Xiang,[c] Zikang Tang,[c] Hao Yu,*[a] and Feng Peng*[a]

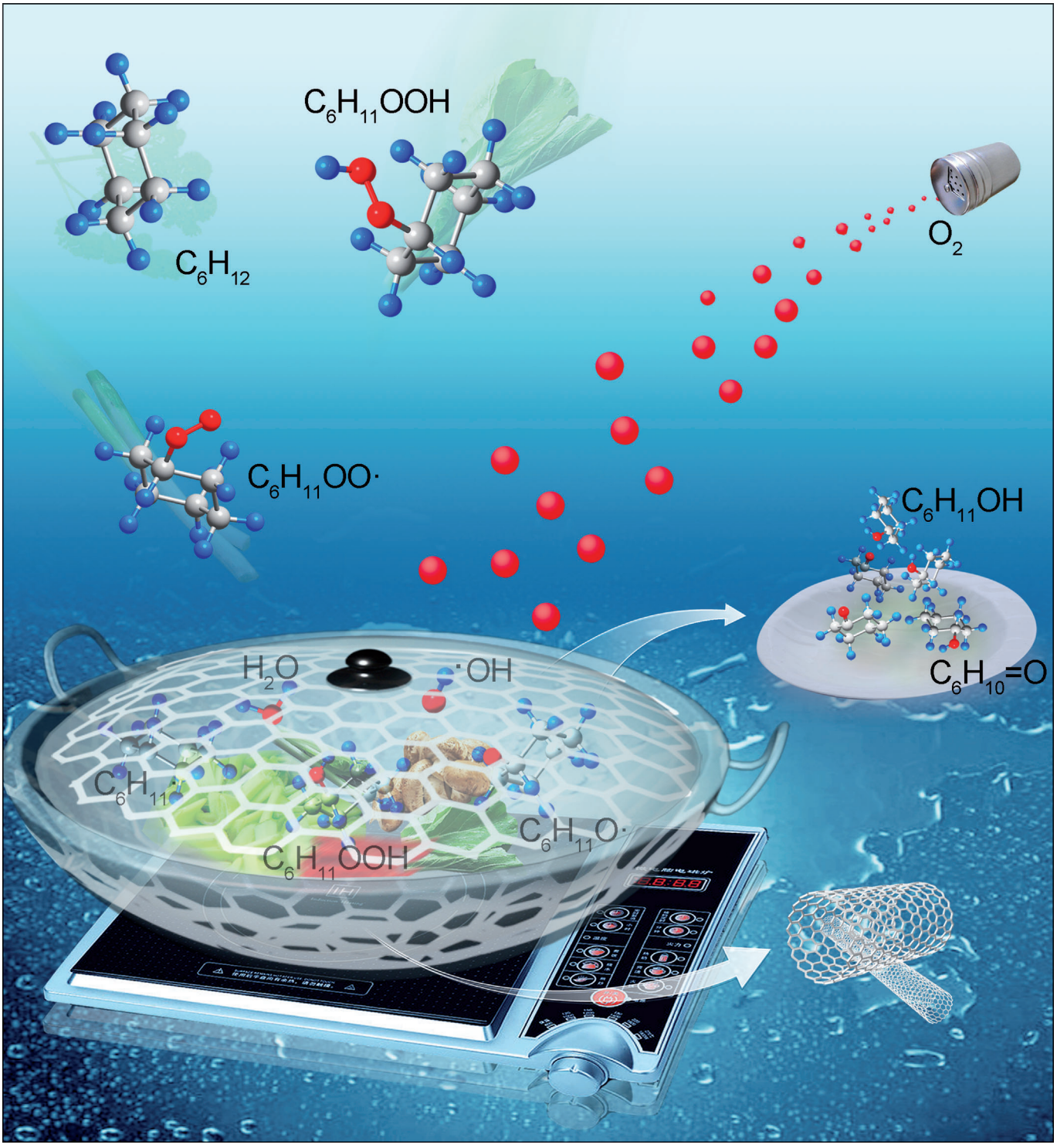

Abstract: As some of the most interesting metal-free catalysts, carbon nanotubes (CNTs) and other carbon-based nanomaterials show great promise for some important chemical reactions, such as the selective oxidation of cyclohexane (C_6H_{12}). Due to the lack of fundamental understanding of carbon catalysis in liquid-phase reactions, we have sought to unravel the role of CNTs in the catalytic oxidation of C_6H_{12} through a combination of kinetic analysis, in situ spectroscopy, and density functional theory. The catalytic effect of CNTs originates from a weak interaction between radicals and their graphene skeletons, which confines the radicals around their surfaces. This, in turn, enhances the electron-transfer catalysis of peroxides to yield the corresponding alcohol and ketone.

Keywords: carbon nanotubes · charge transfer · cyclohexane oxidation · in situ spectroscopy · reaction mechanisms

Introduction

Carbon-based nanomaterials, including fullerenes, carbon nanotubes (CNTs), carbon nanofibers, graphenes, nano-diamonds, and their composites, show great promise as metal-free catalysts in a wide spectrum of important reactions, such as the oxidative dehydrogenation (ODH) of hydrocarbons,[1] the oxygen reduction reaction,[2] the selective oxidation of alcohols,[3] and so on (for more applications, see recent reviews[4]). They are superior to traditional metal catalysts due to their unique electronic structures, surface functionalities, environmentally benign nature, recyclability, and low cost. In the last decade, considerable effort has been directed towards unraveling the catalytic roles of carbon-based materials so as to enable the rational design of the next-generation metal-free catalysts. Hitherto, several catalytic modes of carbon have been identified. In gas-phase ODH reactions, the catalytic cycle starts with the activation and dehydrogenation of hydrocarbons at quinone sites, and ends with the re-activation of carbon by oxygen.[1b,5] At lower temperatures, epoxide C–O–C species may be responsible for the dissociation and insertion of oxygen in selective oxidations.[3a,6] Defects in the carbon-based nanomaterials allow for the activation of methane, which involves the absorption of carbon atoms and the release of hydrogen.[7] In particular, dopants in the carbon skeleton play important roles in tuning the electronic characteristics. For instance, N atoms induce more positive charge on the adjacent carbon atoms, thus facilitating oxygen dissociation in the oxygen reduction reaction.[2b,8] However, so far, the mechanistic picture of carbon catalysis in most liquid-phase reactions remains either unclear or controversial.

Recently, excellent catalytic performances of carbon-based materials in the liquid-phase oxidation of hydrocarbons, an important process in the chemical industry for the production of value-added downstream chemicals, have been demonstrated by several groups.[3a,9] As a representative reaction, the oxidation of C_6H_{12} is used to produce cyclohexanol ($C_6H_{11}OH$) and cyclohexanone ($C_6H_{10}{=}O$) at a level of 10^6 ton y^{-1} for the manufacture of Nylon. The reaction is performed industrially by an autoxidation with oxygen, assisted by homogeneous cobalt or manganese salts.[10] CNTs,[9a] B,N-doped mesocarbons,[9b] and a graphene/C_3N_4 composite[11] have been shown to be active in this reaction. Our recent work has indicated that charge transfer between CNTs and radicals facilitated by delocalized electrons in graphene layers plays a crucial role in the catalysis.[12] However, the lack of fundamental understanding of metal-free catalysis at the molecular level remains the most critical restriction to the further development of liquid-phase hydrocarbon oxidation over carbon materials.

Herein, we present our efforts to unravel the role of CNTs in the catalytic oxidation of C_6H_{12}. By combining kinetic analysis, in situ spectroscopy, and density functional theory (DFT), it has been revealed that the catalysis over CNTs originates from a weak interaction between radicals and graphene skeletons, which confines the radicals around the surfaces of the CNTs. This, in turn, enhances the electron-transfer catalysis of peroxides to yield the corresponding alcohol and ketone.

Results and Discussion

We first conducted a comparative kinetic study of the oxidation of C_6H_{12} with or without a catalyst. Without a catalyst, the liquid-phase oxidation of C_6H_{12} proceeds by a radical autoxidation process.[13] Hermans and co-workers have demonstrated both experimentally[14] and theoretically[15] that hydrogen abstraction by $C_6H_{11}OO^{\bullet}$ is a significant step for chain propagation in the autoxidation of C_6H_{12}. $C_6H_{11}OO^{\bullet}$ abstracts a hydrogen atom from either C_6H_{12} (Scheme 1, S_I

[a] X. Yang, Dr. H. Wang, Prof. H. Yu, Prof. F. Peng
Department of Chemical Engineering
South China University of Technology
Guangzhou 510640 (P.R. China)
Fax: (+86) 20-87114916
E-mail: yuhao@scut.edu.cn
cefpeng@scut.edu.cn

[b] J. Li, Dr. W. Zheng
Department of Applied Chemistry, College of Science
South China Agricultural University
Guangzhou 510642 (P.R. China)

[c] Dr. R. Xiang, Prof. Z. Tang
School of Physics and Engineering
Sun Yat-Sen University
Guangzhou 510275 (P.R. China)

Supporting information for this article is available on the WWW under http://dx.doi.org/10.1002/chem.201300676.

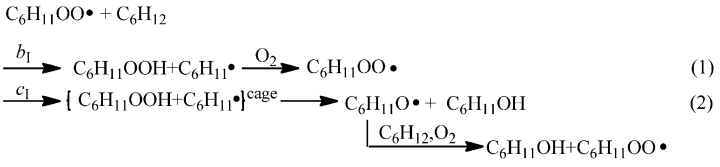

Scheme 1. Reaction pathway involving hydrogen abstraction from C_6H_{12} by $C_6H_{11}OO^{\bullet}$ (S_I route).

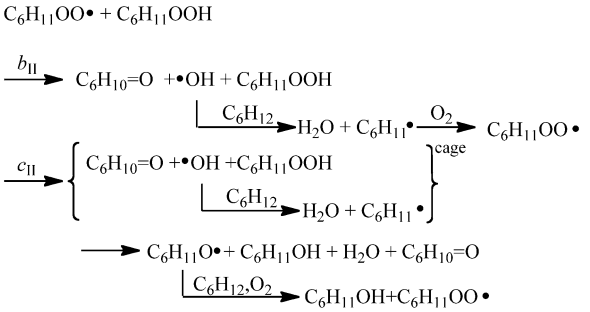

Scheme 2. Reaction pathway involving hydrogen abstraction from $C_6H_{11}OOH$ by $C_6H_{11}OO^{\bullet}$ (S_{II} route).

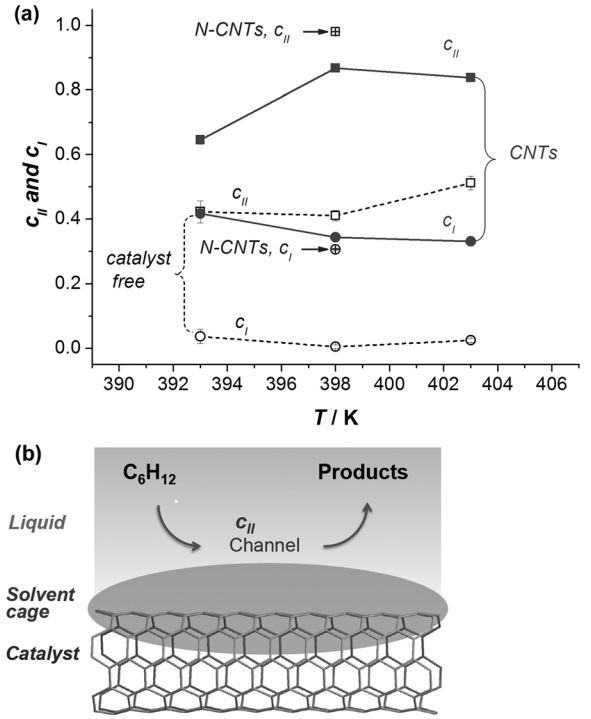

Figure 1. a) Contributions of cage-confined reaction fluxes with/without CNTs/NCNTs as catalysts. b) Schematic diagram of the cage-confined reaction on CNT surfaces. The reaction pathways and parameter definitions are described in Schemes 1 and 2. Reaction conditions: O_2 (1.5 MPa), C_6H_{12} (93.6 g), acetone (64 g), butanone (16.2 g), catalyst (50 mg).

route) or $C_6H_{11}OOH$ (Scheme 2, S_{II} route), with the S_{II} route being much faster. For both of these routes, there are two subsequent reaction pathways, namely the Franck–Rabinowich (F–R) solvent-cage reaction and competing out-of-cage diffusion. Based on a modified kinetic model after Hermans and co-workers,[16] the fractional reaction fluxes in the F–R cage, represented by c_I and c_{II} for the S_I and S_{II} routes, respectively, can be extracted by measuring the product distribution at low conversions (<5%; see the Supporting Information for details).

Assuming that the CNT-catalyzed oxidation involves the same series of elementary steps, the role of the CNTs can be revealed by comparing the key kinetic constants with and without the catalyst. Figure 1 shows the effects of CNTs and N-doped CNTs (NCNTs) on the contributions of cage-confined reaction fluxes. In the catalyst-free case, the fractions of the cage channels of chain propagation reaction fluxes (c_{II} and c_I) were 0.411 and 0.005 at 398 K, respectively. The addition of CNTs impressively increased the c_{II} and c_I values at 398 K to 0.868 and 0.344, respectively. Moreover, the more active NCNTs induced a dominating cage-channel reaction flux for αH abstraction from $C_6H_{11}OOH$, indicated by a c_{II} value of 0.981 at 398 K.

The results suggested that the role of CNTs is equivalent to enhancing the reaction fluxes confined in solvent cages. This provides strong evidence for heterogeneous interface processes. As illustrated in Figure 1b, CNTs may provide solid–liquid interfaces at which reactive intermediates in the solvent cage may be stabilized. A more extensive radical chain would then improve the formation of $C_6H_{11}OH$ and C_6H_{10}=O. Moreover, the participation of carbon surfaces in the cage-channel may result in interactions between carbon and reactive molecules or radicals. We observed a dramatic enhancement of peroxide removal in the presence of carbon, as shown in Figure S2 in the Supporting Information. This suggested that the electron transfer between alkoxyl radicals and the carbon may be facilitated in the cage channel, such that a carbon-catalyzed decomposition of $C_6H_{11}OOH$ was induced in the cages.[17] Due to the much faster kinetics of both the c_{II} and c_I pathways in consuming $C_6H_{11}OOH$, the cage channel dominates the carbon catalysis, especially at low conversions without considering ring opening.

It is interesting to explore the possibility of reaction in the inner space of CNTs as a cage channel. In this work, however, it was unlikely that reaction inside the CNTs played an important role because we used pristine CNTs without further purification. Thus, most of the CNTs were not open-ended and their interiors would not have been accessible to the reactants. This was also indicated by our recent work on NCNTs. It is well known that NCNTs usually show bamboo-like morphology, with compartments separated by graphitic sheets. However, enhanced catalytic activity can be achieved on NCNTs,[9a,18] indicating that the inner surface is unnecessary. Based on these considerations, we neglected the occurrence of reactions in the inner space of the CNTs in this study.

The above kinetic analysis clearly showed a surface-confinement effect of CNTs and their N-doped derivatives. In situ FTIR and Raman spectroscopies were employed to un-

cover the molecular details of the interfacial process. The horizontal attenuated total reflection (HATR) technique was used to monitor the intermediate molecules/radicals stabilized on the surfaces of the CNTs. A ZnSe crystal was uniformly coated with a thin film of CNTs of thickness about 1 μm to guarantee the effective collection of solid–liquid interfacial information (Figure 2a). Strong absorbance bands

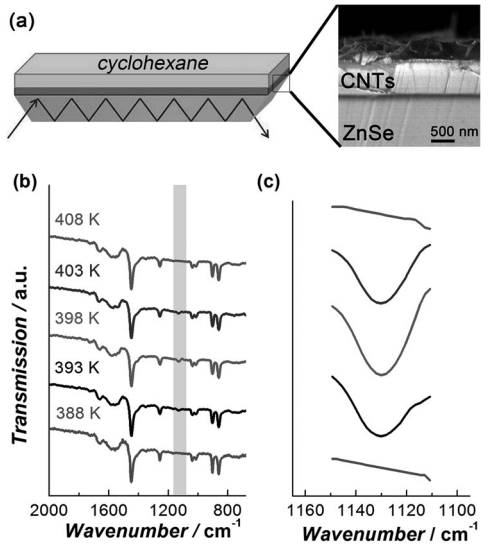

Figure 2. In situ FTIR spectroscopic study of the radical–CNT interaction on the surfaces of CNTs. a) Configuration of the in situ HATR cell. Infrared irradiation is incident through a ZnSe crystal coated with a film of CNTs on the interface with O_2-saturated C_6H_{12}. b) Survey IR spectra in the range 2000–650 cm^{-1} recorded in situ at 388–408 K. c) High-resolution IR spectra in the region 1150–1110 cm^{-1}.

in the range $\tilde{\nu}=3000$–$800\ cm^{-1}$ could be attributed to C–C, C–O, C=O, and C–H_n vibrations (see Figures S3 and S4 in the Supporting Information). After exposing the film to O_2-saturated C_6H_{12}, temperature-dependent IR spectra were recorded in the region $\tilde{\nu}=2000$–$650\ cm^{-1}$ (Figure 2b). On increasing the temperature from 388 to 398 K, a weak signal at $\tilde{\nu}=1130\ cm^{-1}$ emerged and gradually grew, but was then attenuated and disappeared on further heating from 398 to 408 K (see Figure 2c for high-resolution spectra). A set of control experiments was carried out to identify the origin of this peak (see Figure S5in the Supporting Information). It was not observed on CNTs with O_2-saturated benzene, hexane, or toluene, nor on CNTs with N_2-saturated C_6H_{12} within the same temperature range. It was also not detected from O_2-saturated C_6H_{12} without the CNT film (see Figure S6 in the Supporting Information). Thus, it can be assigned as an intrinsic feature reflecting an elementary step of the oxidation of C_6H_{12} on CNTs. Since the signal at $\tilde{\nu}=1130\ cm^{-1}$ is indicative of a stretching vibration of C–O–O bonds in alkyl peroxides,[19] it strongly supports the view that αH abstraction from $C_6H_{11}OOH$ by $C_6H_{11}OO^{\bullet}$ radicals takes place at the interface. The observed peroxide species are likely to be formed in the liquid phase by an initiation process similar to that in the autoxidation, but not by an activation of molecular oxygen on CNTs because the reaction temperature is low. The adsorption of peroxides on CNT surfaces serves as a confinement effect, suppressing the diffusive separation of the reactants and products and thereby enhancing the cage-channel reaction (c_{II}). It was noted that the intensity of the C–O–O vibration was dependent on the reaction temperature. The peak at $\tilde{\nu}=1130\ cm^{-1}$ was only detected in a window from 388 to 408 K. This indicates that the considerable solvent cages at the CNT–liquid interfaces are activated above 393 K, whereas they collapse at higher temperatures due to the accelerated diffusion caused by the extra heat. This observation is consistent with our kinetic experiments. As shown in Figure 1a, the c_{II} value reached a maximum at 398 K and slightly decreased at 403 K, indicating a greater contribution from the competing diffusive separation route at higher temperatures.

Besides the stabilization effect, an interaction between CNTs and intermediate molecules/radicals in the cages can be expected. We have previously emphasized that electron transfer on CNTs plays a key role.[9a,12] In this work, electron transfer was monitored by in situ Raman spectroscopy, as shown in Figure 3a. Due to the spectroscopic sensitivity of their electronic structure, single-walled CNTs (SWCNTs) were adopted for the in situ Raman study. High-purity (>99%) vertically aligned SWCNTs were grown on a silica substrate by catalytic chemical vapor deposition using ethanol[20] (Figure 3a; see Figure S7 in the Supporting Information for TEM and top-view SEM images). As shown in Figure 3b, the intensity of the G-band decreased under the working conditions of C_6H_{12} oxidation, as a consequence of

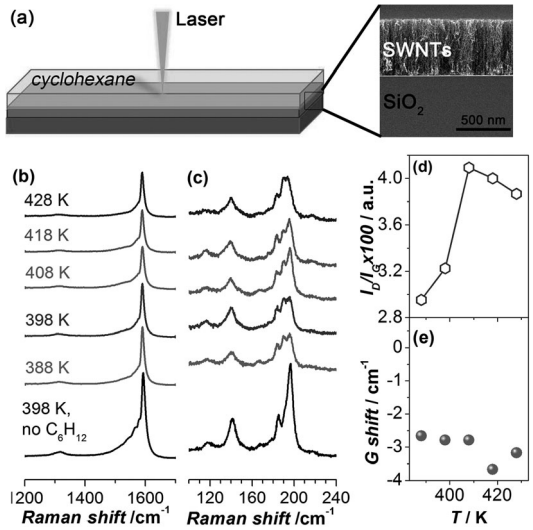

Figure 3. In situ Raman spectroscopic study of electron transfer on the surfaces of CNTs. a) Configuration of the in situ Raman cell. An array of vertically aligned SWCNTs was grown at the interface between SiO_2 and O_2-saturated C_6H_{12}. b) G and D bands of SWCNTs recorded in situ at 388–428 K by using a 633 nm laser. c) RBM modes of SWCNTs recorded in situ at 388–428 K by using a 633 nm laser. The Raman spectrum of a bare SWCNT array at 398 K is also shown in b) and c) for comparison. d) Evolution of I_D/I_G values with reaction temperature. e) The shift of the G band frequency relative to that of bare SWCNTs at 398 K.

the electron density variation caused by the attack of charged radicals. The attack could either add electrons to an empty van Hove singularity, or remove electrons from a filled van Hove singularity. Hence, the SWCNTs underwent weaker optical transitions with resonant photons and showed weaker Raman intensities.[21] This was also manifested by a loss of intensity of the radial breathing mode (RBM; see Figure 3c), especially for the high-frequency peak at $\tilde{\nu}=197\,cm^{-1}$, since the thinner SWCNTs are more susceptible to attack. In addition, with O_2-saturated C_6H_{12}, the Raman tangential G-band showed a frequency downshift of about $3\,cm^{-1}$ (see Figure 3e), due to the injection of electrons from the radicals to the SWCNTs.[22] The interaction with radicals also altered the intensity ratio of the D and G bands. As shown in Figure 3d, the I_D/I_G ratio increased with temperature from 388 to 408 K, reflecting the fact that the activated solvent cages increased the likelihood of radical attack. However, the I_D/I_G ratio gradually decreased above 408 K, reiterating the competitive diffusive separation of species from the cages, as revealed by the kinetic and in situ IR studies. Similar results were obtained by using multi-walled CNTs as catalysts (see Figure S8 in the Supporting Information). It should be noted that the discrepancy between the temperatures at which the IR intensities or I_D/I_G ratios reached their maximum values by Raman and IR spectroscopies implied different mechanisms. The increase in I_D/I_G was caused by radical attack, which can occur either in solvent cages near the surface or in the liquid phase. Since a higher temperature favors attack from the liquid phase, the highest I_D/I_G ratio was observed at 408 K, slightly higher than that of the maximum of the IR band, at which the solvent cages near the surfaces of CNTs tend to disintegrate. It is worth mentioning that the RBM and G bands could be completely recovered after suitable temperature programming (see Figure S9 in the Supporting Information), indicating a reversible interaction between the radicals and CNTs. Thus, the role of CNTs is to trap reactants/products to form surface-confined solvent cages in which electron transfer between radicals and CNTs is facilitated, without forming defects or strong chemical bonds.

The nature of the interaction was further explored by DFT calculations. Figure 4 shows the optimized structures of radical–SWCNT supramolecular complexes and their formation energies. Two key radicals, $C_6H_{11}OO^{\bullet}$ and $C_6H_{11}^{\bullet}$, were investigated to represent the species in our kinetic model. About $1\,kcal\,mol^{-1}$ will be released upon the formation of these complexes. This indicates that the interaction is unlikely to involve a strong chemical adsorption between the radicals and CNTs, but rather a type of weak interaction, such as the electrostatic interaction. This result is consistent with that of the Raman study, corroborating that the radical attack and charge transfer between catalysts and radicals do not irreversibly generate defects. Nevertheless, the weak adsorption results in a fivefold activity improvement of the oxidation reaction compared to the blank control experiment, as detailed in our previous work.[9a] In particular, this interaction nicely explains the catalytic enhancement seen upon

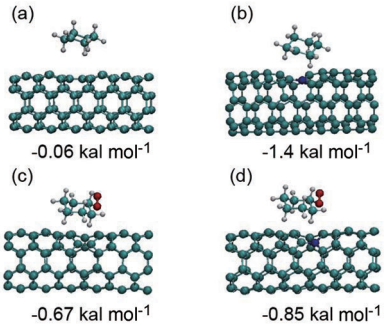

Figure 4. Optimized structures of the supramolecular complexes: a) $C_6H_{11}^{\bullet}$–SWCNT, b) $C_6H_{11}^{\bullet}$–*N*-SWCNT, c) $C_6H_{11}OO^{\bullet}$–SWCNT, and d) $C_6H_{11}OO^{\bullet}$–*N*-SWCNT. The CNT model is a (4,4) armchair nanotube. The formation energy (E_f) is defined as the total energy (E_{tot}) gained by the adsorption of a molecule at equilibrium distance: $E_f = E_{tot}(\text{tube+molecule}) - E_{tot}(\text{tube}) - E_{tot}(\text{molecule})$.[23] Cyan: carbon; white: hydrogen; red: oxygen; blue: nitrogen.

nitrogen doping. Introducing one nitrogen atom into the lattice of an SWCNT, the formation energies for $C_6H_{11}^{\bullet}$–SWCNT and $C_6H_{11}OO^{\bullet}$–SWCNT decrease from -0.06 to $-1.4\,kcal\,mol^{-1}$ and from -0.67 to $-0.85\,kcal\,mol^{-1}$, respectively, on an N-SWCNT. The calculations demonstrated that nitrogen doping effectively decreases the adsorption barrier for $C_6H_{11}^{\bullet}$, one of the major radicals involved in the cage-channel reaction flux. Although the adsorption is weak, it may considerably enhance the electron transfer between CNTs and radicals, due to the large rate constants of electron-transfer reactions.[24]

Conclusion

To summarize, the catalytic mechanism underpinning the metal-free CNT-catalyzed oxidation of C_6H_{12} with molecular oxygen in the liquid phase has been unraveled at the molecular level by analyzing product distributions, in situ monitoring of catalyst surfaces, and theoretical calculations. CNTs play a key role in the propagation of the radical chain reaction, through effectively promoting the reaction flux in solvent cages. The formation of peroxide intermediates confined at CNT surfaces has been demonstrated by an in situ FTIR investigation, emphasizing the heterogeneous nature of the radical-based carbon catalysis. At the solid–liquid interface, electron transfer between radicals and CNTs is facilitated, thus enhancing the efficiency of the cage reaction yielding the ketone and alcohol products. The mechanistic insights presented here provide the first detailed understanding of the promising carbon catalysis in the liquid phase at the molecular level. We believe that it will aid more rational design for the emerging carbon catalysis and shed light on the relevant carbon-catalyzed processes in the liquid phase.

Experimental Section

Synthesis: Multi-walled CNTs, with outer diameters of about 10–20 nm and inner diameters of 5–10 nm, were produced by a chemical vapor deposition (CVD) method using liquefied petroleum gas as the carbon source over an Fe–Mo/Al_2O_3 catalyst[25] in a horizontal tubular quartz furnace of inner diameter 4 cm. Before the growth of the CNTs, the catalyst was activated with a mixture of H_2 and N_2 (both at 25 N cm^3 min^{-1}) for 30 min. The CNTs were grown at 700 °C for 130 min, with 20 N cm^3 min^{-1} liquefied petroleum gas, 10 N cm^3 min^{-1} H_2, and 50 N cm^3 min^{-1} N_2. N-doped CNTs were synthesized by the same CVD method, but with aniline as the carbon source in an NH_3 atmosphere. Aniline (10 mL) was injected by means of a syringe pump at a rate of 3 mL h^{-1} and was vaporized in the quartz tube at 180 °C. The flow rate of NH_3 was 500 N cm^3 min^{-1}. The SWCNT arrays used in this work were synthesized by a catalytic CVD method using ethanol developed by Maruyama and co-workers.[20a,26] In brief, cobalt and molybdenum nanoparticles were loaded onto a quartz substrate by a liquid-based dip-coating method. Subsequently, the catalytic quartz substrate was subjected to CVD with low-pressure ethanol vapor at 800 °C. The Brunauer–Emmett–Teller specific surface areas of the CNTs and NCNTs were 127.8 and 155.1 m^2 g^{-1}, respectively. About 4.36 at % nitrogen was incorporated into the NCNTs, with 38.8 % quaternary and 28.1 % pyridinic nitrogen (for more details about the structure of NCNTs, see elsewhere[18]).

In situ spectroscopic experiments: For the in situ IR experiments, a trapezoidal ZnSe internal reflection element of thickness 2 mm was coated with a layer of catalyst of around 1 μm by dropping and vacuum volatizing a solution of the CNTs in cyclohexanol. HATR-IR spectra were recorded on a Nicolet 6700 spectrometer equipped with a commercial HATR-IR unit (Harrick HATR). The spectra were obtained by accumulating 200 scans at a resolution of 4 cm^{-1}. Raman spectra were obtained on a LabRAM Aramis micro Raman spectrometer under excitation with a 633 nm laser of spot size 2 μm. In situ HATR-IR and Raman experiments were carried out by contacting the catalysts with cyclohexane saturated with O_2. The cyclohexane was saturated with O_2 at 1 MPa in an autoclave, then immediately transferred to the in situ cells. The in situ spectra were collected after the required experimental conditions had been maintained in a steady state for 1 min.

Catalytic tests: Cyclohexane oxidation reactions were carried out in batch mode in a mechanically stirred (1500 rpm) 300 mL Parr autoclave. Prior to the experiments, the reactor wall was passivated with a saturated sodium pyrophosphate solution. Before each reaction, the reactants along with butanone as an internal standard, acetone as solvent, and the catalyst were loaded into the autoclave and the reactor was flushed with N_2. It was heated to a stable operational temperature, whereupon pure O_2 was introduced, defining $t=0$. The products were analyzed by gas chromatography (GC). GC was used to analyze the concentrations of cyclohexane, cyclohexanol, and cyclohexanone with reference to the butanone internal standard. The concentration of cyclohexyl hydroperoxide was analyzed by reducing it to cyclohexanol with triphenylphosphine. GC conditions: DB-5 MS capillary column (30 m, DF = 0.25 μm, 0.25 mm i.d.), FID detector, injector temperature 280 °C, and oven temperature 90 °C. The carbon balance was better than 95 % by the described analytical procedure.

DFT calculations: All calculations were performed by using the Vienna ab initio simulation package (VASP).[27] The non-local exchange-correlation energy was evaluated by using the Perdew–Burke–Ernzehof function.[28] A plane-wave basis set with a cut-off energy of 400 eV was used. *k*-Point sampling was restricted to a single point. The unit cell dimensions were 18 × 18 × 14.8 Å. Models used in this work were (4,4) armchair nanotubes with Stone–Wales defects.

Acknowledgements

This work was supported by the National Science Foundation of China (Nos. 21133010, 21273079, 51002190), the Guangdong Provincial National Science Foundation of China (Nos. 9251064101000020, S20120011275), and the Program for New Century Excellent Talents in University (NCET-12–0190).

[1] a) N. Keller, N. I. Maksimova, V. V. Roddatis, M. Schur, G. Mestl, Y. V. Butenko, V. L. Kuznetsov, R. Schlögl, *Angew. Chem.* **2002**, *114*, 1962–1966; *Angew. Chem. Int. Ed.* **2002**, *41*, 1885–1888; b) J. Zhang, X. Liu, R. Blume, A. Zhang, R. Schlögl, D. S. Su, *Science* **2008**, *322*, 73–77.

[2] a) Z.-W. Liu, F. Peng, H.-J. Wang, H. Yu, W.-X. Zheng, J. Yang, *Angew. Chem.* **2011**, *123*, 3315–3319; *Angew. Chem. Int. Ed.* **2011**, *50*, 3257–3261; b) K. Gong, F. Du, Z. Xia, M. Durstock, L. Dai, *Science* **2009**, *323*, 760–764.

[3] a) D. R. Dreyer, H.-P. Jia, C. W. Bielawski, *Angew. Chem.* **2010**, *122*, 6965–6968; *Angew. Chem. Int. Ed.* **2010**, *49*, 6813–6816; b) J. Luo, F. Peng, H. Yu, H. Wang, *Chem. Eng. J.* **2012**, *204–206*, 98–106.

[4] a) Y. Wang, X. Wang, M. Antonietti, *Angew. Chem. Int. Ed.* **2012**, *51*, 68–89; b) D. Yu, E. Nagelli, F. Du, L. Dai, *J. Phys. Chem. Lett.* **2010**, *1*, 2165–2173; c) D. S. Su, J. Zhang, B. Frank, A. Thomas, X. Wang, J. Paraknowitsch, R. Schlögl, *ChemSusChem* **2010**, *3*, 169–180.

[5] a) M. F. R. Pereira, J. J. M. Órfão, J. L. Figueiredo, *Appl. Catal. A* **2001**, *218*, 307–318; b) J. A. Maciá-Agulló, D. Cazorla-Amorós, A. Linares-Solano, U. Wild, D. S. Su, R. Schlögl, *Catal. Today* **2005**, *102–103*, 248–253; c) J. Zhang, X. Wang, Q. Su, L. Zhi, A. Thomas, X. Feng, D. S. Su, R. Schlögl, K. Müllen, *J. Am. Chem. Soc.* **2009**, *131*, 11296–11297.

[6] a) B. Frank, R. Blume, A. Rinaldi, A. Trunschke, R. Schlögl, *Angew. Chem.* **2011**, *123*, 10408–10413; *Angew. Chem. Int. Ed.* **2011**, *50*, 10226–10230; b) D. W. Boukhvalov, D. R. Dreyer, C. W. Bielawski, Y.-W. Son, *ChemCatChem* **2012**, *4*, 1844–1849.

[7] a) N. Muradov, F. Smith, A. T-Raissi, *Catal. Today* **2005**, *102–103*, 225–233; b) S. Y. Lee, J. H. Kwak, G. Y. Han, T. J. Lee, K. J. Yoon, *Carbon* **2008**, *46*, 342–348.

[8] R. Liu, D. Wu, X. Feng, K. Müllen, *Angew. Chem.* **2010**, *122*, 2619–2623; *Angew. Chem. Int. Ed.* **2010**, *49*, 2565–2569.

[9] a) H. Yu, F. Peng, J. Tan, X. Hu, H. Wang, J. Yang, W. Zheng, *Angew. Chem.* **2011**, *123*, 4064–4068; *Angew. Chem. Int. Ed.* **2011**, *50*, 3978–3982; b) Y. Wang, J. Zhang, X. Wang, M. Antonietti, H. Li, *Angew. Chem.* **2010**, *122*, 3428–3431; *Angew. Chem. Int. Ed.* **2010**, *49*, 3356–3359.

[10] U. Schuchardt, D. Cardoso, R. Sercheli, R. Pereira, R. S. da Cruz, M. C. Guerreiro, D. Mandelli, E. V. Spinacé, E. L. Pires, *Appl. Catal. A* **2001**, *211*, 1–17.

[11] X.-H. Li, J.-S. Chen, X. Wang, J. Sun, M. Antonietti, *J. Am. Chem. Soc.* **2011**, *133*, 8074–8077.

[12] X. Yang, H. Yu, F. Peng, H. Wang, *ChemSusChem* **2012**, *5*, 1213–1217.

[13] S. Bhaduri, D. Mukesh in *Homogeneous Catalysis*, Wiley, New York, **2000**.

[14] I. Hermans, P. A. Jacobs, J. Peeters, *J. Mol. Catal. A: Chem.* **2006**, *251*, 221–228.

[15] I. Hermans, T. L. Nguyen, P. A. Jacobs, J. Peeters, *ChemPhysChem* **2005**, *6*, 637–645.

[16] I. Hermans, P. A. Jacobs, J. Peeters, *Chem. Eur. J.* **2006**, *12*, 4229–4240.

[17] P. S. Engel, W. E. Billups, D. W. Abmayr, K. Tsvaygboym, R. Wang, *J. Phys. Chem. C* **2008**, *112*, 695–700.

[18] Y. Cao, H. Yu, J. Tan, F. Peng, H. Wang, J. Li, W. Zheng, N.-B. Wong, *Carbon* **2013**, *57*, 433–442.

[19] J. A. Dean, *Analytical Chemistry Handbook*, McGraw–Hill, New York, **1995**.

[20] a) S. Maruyama, R. Kojima, Y. Miyauchi, S. Chiashi, M. Kohno, *Chem. Phys. Lett.* **2002**, *360*, 229–234; b) R. Xiang, T. Wu, E. Einarsson, Y. Suzuki, Y. Murakami, J. Shiomi, S. Maruyama, *J. Am. Chem. Soc.* **2009**, *131*, 10344–10345.

[21] a) P. Umek, J. W. Seo, K. Hernadi, A. Mrzel, P. Pechy, D. D. Mihailovic, L. Forró, *Chem. Mater.* **2003**, *15*, 4751–4755; b) A. Mukherjee,

R. Combs, J. Chattopadhyay, D. W. Abmayr, P. S. Engel, W. E. Billups, *Chem. Mater.* **2008**, *20*, 7339–7343.
[22] a) A. M. Rao, P. C. Eklund, S. Bandow, A. Thess, R. E. Smalley, *Nature* **1997**, *388*, 257–259; b) M. Shim, T. Ozel, A. Gaur, C. Wang, *J. Am. Chem. Soc.* **2006**, *128*, 7522–7530; c) P. Corio, A. Jorio, N. Demir, M. S. Dresselhaus, *Chem. Phys. Lett.* **2004**, *392*, 396–402.
[23] J. Zhao, J. P. Lu, J. Han, C.-K. Yang, *Appl. Phys. Lett.* **2003**, *82*, 3746–3748.
[24] M. Bietti, G. A. DiLabio, O. Lanzalunga, M. Salamone, *J. Org. Chem.* **2010**, *75*, 5875–5881.
[25] W. Z. Qian, H. Yu, F. Wei, Q. F. Zhang, Z. W. Wang, *Carbon* **2002**, *40*, 2968–2970.
[26] a) Y. Murakami, Y. Miyauchi, S. Chiashi, S. Maruyama, *Chem. Phys. Lett.* **2003**, *377*, 49–54; b) Y. Murakami, S. Chiashi, Y. Miyauchi, M. Hu, M. Ogura, T. Okubo, S. Maruyama, *Chem. Phys. Lett.* **2004**, *385*, 298–303; c) S. Maruyama, E. Einarsson, Y. Murakami, T. Edamura, *Chem. Phys. Lett.* **2005**, *403*, 320–323.
[27] G. Kresse, J. Hafner, *Phys. Rev. B* **1993**, *48*, 13115–13118.
[28] J. P. Perdew, K. Burke, M. Ernzerhof, *Phys. Rev. Lett.* **1996**, *77*, 3865–3868.

Received: February 21, 2013
Published online: June 20, 2013

